Phase Behavior of Polystyrene in Methyl Acetate: A Static Light Scattering Study

A. Wakker,* F. van Dijk, and M. A. van Dijk

Koninklijke/Shell-Laboratorium, Amsterdam (Shell Research B.V.), Badhuisweg 3, 1031 CM Amsterdam, The Netherlands

Received January 28, 1993; Revised Manuscript Received June 9, 1993

ABSTRACT: The phase behavior of a model polymer solution, polystyrene in methyl aceate, has been investigated by means of static light scattering. Rayleigh ratios and correlation lengths have been measured over a broad range of temperatures (300–400 K) and concentrations (0.5–10.3 wt %). A novel procedure to correct the measured forward scattered intensity for turbidity has been applied. Rayleigh ratios have been used to determine values of the free energy curvature ($\partial^2\Delta G/\partial c^2$) in the homogeneous one-phase region of this system, i.e., between the upper and lower critical phase boundaries. The complete data set forms a unique basis which can be used to test thermodynamic model predictions.

Introduction

Since the pioneering work of Flory[1,2] and Huggins,[3–5] a vast number of experimental studies on the phase behavior of simple model polymer solutions have been published. In these studies, one observes phase separation phenomena associated with upper critical demixing (phase separation upon cooling) or lower critical demixing (phase separation upon heating). One measures either cloud point curves,[6–14] which are the loci of points where the chemical potentials of the constituents in both phases are equal, or spinodal curves,[15–18] which are located inside the metastable two-phase region, separating the metastable from the unstable phase. Hence, spinodal curves are defined as the loci of points where the free energy curvature is zero.

Many attempts have been made to predict the observed phase behavior. Nowadays, it is well recognized that in nonpolar polymer solutions without specific interactions dispersion forces and compressibility effects are the driving forces behind upper and lower critical demixing, respectively.[19–26] In systems with strong specific interactions, upper critical demixing is usually not observed. Lower critical demixing however does occur, and it is driven by the entropy loss associated with the formation of directional-specific interactions.[27–29] The situation becomes more complicated in weakly polar solutions: both compressibility effects and specific interactions may have to be taken into account in describing the actual phase behavior.[30]

Although the phase behavior of a polymer solution can be described by various thermodynamic models, we are not yet at the point where phase behavior can be predicted by using independent a priori information. This is partly due to the fact that all available models are based on mean field lattice–gas theories, which are inadequate in describing the actual structure and interactions in a real polymer solution. However, it should be noted that cloud points and spinodals, which are in general the only experimental data available, reflect only a minor part of the complete free energy of mixing "phase space". Hence, these types of data are of rather limited use for testing thermodynamic model predictions.

A better way to proceed experimentally is to measure directly the free energy curvature as a function of temperature and concentration, preferably in the complete homogeneous one-phase region of the solution. This we have done, and we will present the results of a static light scattering study on the thermodynamic behavior of polystyrene in methyl acetate. This system is chosen because it undergoes phase separation both upon cooling (upper critical solution temperature, UCST ~ 300 K) and upon heating (lower critical solution temperature, LCST ~ 400 K) in an experimentally accessible temperature range. Hence, all features of polymer solution phase behavior are expected to be present.

In previous work, Chu et al. investigated the collapse transitions of dilute solutions of very high molecular weight (M_w = 2000–8300 kg/mol) polystyrene in methyl acetate at the upper and lower critical Θ temperatures.[31] Light scattering data from a low molecular weight (M_w = 179 kg/mol) solution, measured in the off-critical region, have been used to determine, among other things, values of the osmotic second virial coefficients.[32] This allowed a qualitative description of the phase behavior.

In this work, the complete phase behavior of dilute to moderately concentrated solutions (up to 10.3% by weight fraction) of high molecular weight polystyrene (M = 770 kg/mol) in methyl acetate will be determined quantitatively. Light scattering data will be used to generate values for $\partial^2\Delta G/\partial c^2$, the second derivative of the Gibbs free energy of mixing with respect to concentration, in the homogeneous one-phase region of this system, including the critical region. To generate these data, it is necessary to handle the large scattering intensities (turbidity) of critical and concentrated polymer solutions. We will derive a numerical procedure to calculate the actual forward scattered intensity from the measured forward scattering intensity and the angular dependence. This method can be applied to every system in which turbidity plays a role and in which multiple scattering can still be neglected.

The quantification of free energy curvatures $\partial^2\Delta G/\partial c^2$ as a function of temperature and composition is the principal result of this work. Since the phase behavior is completely governed by the free energy curvature, the complete data set forms a unique basis to allow for a comparison with theoretical models.

Static Light Scattering from Polymer Solutions

Relation with Free Energy Curvature. We consider the usual geometry for the light scattered from a cylindrical cuvette, where the incident beam is vertically polarized and where the light is detected in the horizontal plane

* Author to whom correspondence should be addressed. Present address: Chemical Research Centre, Shell Louvain-la-Neuve (Shell Research S.A.), Avenue Jean Monnet 1, B-1348 Ottignies-Louvain-la-Neuve, Belgium.

0024-9297/93/2226-5088$04.00/0 © 1993 American Chemical Society

perpendicular to the polarization vector of the incident beam. In this geometry, the general formula for the angle-dependent intensity $I(q(\theta))$ is given by[33]

$$I(q(\theta)) = K(V^2/R_d^2)\langle\delta\epsilon(q)^2\rangle I_0 \quad (1)$$

where $K = (2\pi/\lambda)^4(1/16\pi^2) = \pi^2/\lambda^4$ (λ is the wavelength in vacuum), I_0 is the intensity of the primary light beam, and R_d is the distance from the scattering volume to the detector. Formally, V is a volume element associated with the fluctuation in the dielectric constants $\delta\epsilon(q)$. $q = (4\pi/\lambda)n_s \sin(\theta/2)$ is the wave vector change in the scattering event,[33] where n_s is the refractive index of the solution and θ is the scattering angle.

We define the Rayleigh ratio $R(q(\theta))$ as the ratio of the scattered intensity to the primary beam intensity multiplied by R_d^2/V:

$$R(q(\theta)) = I(q)R_d^2/(VI_0) = KV\langle\delta\epsilon(q)^2\rangle \quad (2)$$

$R(q(\theta))$ denotes the relative scattered intensity per unit scattering volume scattered in a unit solid angle in the direction θ.

In a multicomponent system, fluctuations in ϵ are coupled to fluctuations in concentration c (kg/m^3) and density ρ (kg/m^3). We only consider the contribution from concentration fluctuations to light scattering. The minor contribution from density fluctuations can be taken into account by subtraction of the pure solvent scattering intensity. The expression for the Rayleigh ratio becomes

$$R(q(\theta)) = KV\left(\frac{\partial\epsilon}{\partial c}\right)^2\langle\delta c(q)^2\rangle \quad (3)$$

$$= 4KVn_s^2\left(\frac{\partial n_s}{\partial c}\right)^2\langle\delta c(q)^2\rangle \quad (4)$$

The fluctuation theory of Einstein and Smoluchowski[34,35] connects the amplitude of concentration fluctuations $\langle\delta c(q)^2\rangle$ with the Gibbs free energy curvature $\partial^2\Delta G/\partial c^2$. In the limit $q \to 0$ we can write

$$\lim_{q\to 0}\langle\delta c(q)^2\rangle \equiv \langle\delta c(0)^2\rangle = k_BT\left[\frac{\partial^2\Delta G}{\partial c^2}\right]^{-1} \quad (5)$$

which gives

$$\lim_{q\to 0} R(q(\theta)) \equiv R(q(0)) = 4KVn_s^2\left(\frac{\partial n_s}{\partial c}\right)_T^2 k_BT\left[\frac{\partial^2\Delta G}{\partial c^2}\right]^{-1} \quad (6)$$

Since the free energy curvature is associated with the volume element V, eq 6 can be rewritten as

$$R(q(0)) = 4Kn_s^2\left(\frac{\partial n_s}{\partial c}\right)_T^2 k_BT\left[\frac{\partial^2\Delta G^V}{\partial c^2}\right]^{-1} \quad (7)$$

where ΔG^V is the Gibbs free energy per unit volume.

Structure Factor $S(q)$. To describe the angular dependence of light scattering from polymer solutions, we define the static structure factor $S(q)$:

$$S(q) \equiv \frac{R(q(\theta))}{R(q(0))} \quad (8)$$

Obviously, $S(\theta=0) \equiv 1$.

For dilute polymer solutions, all angular dependence of $S(q)$ comes from the interference within single polymer chains, and in that case $S(q)$ reduces to the single particle form factor $P(q)$:[33]

$$S(q) = P(q) = 1 - (1/3)R_g^2q^2 + \ldots \quad (9)$$

where R_g is the radius of gyration of a single polymer chain. This description is not value for more concentrated solutions where polymer coils interact and where the structure of the solution becomes more continuous.

It can be seen from eq 7 that the zero-angle Rayleigh ratio diverges when the curvature of the free energy surface becomes zero (which defines the so-called spinodal curve). This phenomenon, well known as critical opalescence,[36] is accompanied by long-range concentration fluctuations with correlation length ξ. These fluctuations occur because, on a microcopic scale, the thermodynamic driving force that drives small concentration fluctuations back to homogeneity vanishes at the spinodal ($\partial^2\Delta G/\partial c^2 = 0$). Hence, close to spinodals, the structure factor must be described in terms of long-range correlations rather than as a single-particle form factor. An analytical expression for the structure factor $S(q)$ close to spinodals has been given by Ornstein and Zernike:[36]

$$S(q) = \frac{1}{1 + \xi^2q^2} \quad (10)$$

Note that in expanded form, eqs 9 and 10 have the same q dependence, provided that $(1/3)R_g^2q^2 \ll 1$, so that the higher moments in eq 9 can be neglected.[33] In our case, where we are dealing with not too high a molecular weight polymer ($R_g \approx 25$ nm; $R_g^2q^2 \approx 0.04$) this condition is fulfilled (as will be shown). In effect, this means that any $S(q)$, either single particle or long range in nature, can be written in the form of the Lorentzian profile, eq 10.

Turbidity. The large turbidity τ, that is, the Rayleigh ratio integrated over the complete solid angle Ω, of concentrated or critical polymer solutions will lead to a measurable attenuation of the laser beam. Hence, effects of turbidity will have to be taken into account in analyzing our light scattering data. The light scattering takes place in a scattering volume at the center of a cylindrical cuvette with diameter d. Before entering the scattering volume, the intensity of the incident beam will be attenuated by a factor $\exp(-\tau d/2)$. On leaving the cuvette, the scattered light will be attenuated again by the same factor. Hence, the measured Rayleigh ratio R_m is related to the actual Rayleigh ratio R by

$$R_m = R\exp(-\tau d) \quad (11)$$

for any scattering angle.

For anisotropic scatterers the expression for τ can only be solved when the angular dependence of the Rayleigh ratio is known. As discussed above, we assume that eq 10 can be used as a general expression for the structure factor $S(q)$, if ξ is regarded as an arbitrary parameter. Hence, we can write:

$$\tau = R(q(0))\int d\Omega\, S(q)\sin^2\varphi$$

$$= R(q(0))\int d\Omega\frac{\sin^2\varphi}{1 + \xi^2q^2} \quad (12)$$

where the $\sin^2\varphi$ term comes from the symmetry of the dipole radiation tensor.[33] φ is the angle between the vertical polarization vector of the laser beam and the

scattering vector. It is easy to show that eq 12 can be written as follows:[37]

$$\tau = \frac{R(q(0))}{2k_i^2\xi^2}\int d\Omega \frac{\sin^2\varphi}{\alpha - \cos\theta} \tag{13}$$

where α is defined as

$$\alpha = 1 + \frac{1}{2k_i^2\xi^2} \tag{14}$$

An analytical solution of eq 13 exists:[37]

$$\tau = \frac{R(q(0))\pi}{2k_i^2\xi^2}\left[(1+\alpha^2)\ln\left[\frac{\alpha+1}{\alpha-1}\right] - 2\alpha\right] \tag{15}$$

Equation 15 reduces to the correct limit $8R(q(0))\pi/3$ when $\xi \to 0$. We now have an expression for τ as a function of $R(q(0))$ and ξ, so that we can write

$$R(q(0))_m = R(q(0))\exp[-\tau(R(q(0)),\xi)d] \tag{16}$$

Given the fact that both $R(q(0))_m$ and ξ can be determined experimentally, the actual Rayleigh ratio $R(q(0))$ can be solved numerically from eq 16. We shall use eq 16 to correct our $R(q(0))_m$ data for turbidity.

Experimental Section

Light Scattering. The static light scattering experiments were performed with an automatic goniometer with appurtenant hardware and optics (from ALV Laservertriebsges., mbH), which can be accurately aligned for static measurements using a procedure adopted from Bantle et al.[38] The laser used was an argon ion laser operating at a wavelength of 514.5 nm at a power of 200 mW, which allows very rapid measurement. The setup is equipped with a special high-temperature ceramic light scattering cell housing. It is constructed in such a way that no significant temperature gradients are present inside the light scattering cuvette, which prevents both convection inside the cuvette and refraction of the laser beam. Below 370 K, toluene is used as the refractive index matching liquid, and above 370 K, dodecane is used. We briefly summarize the process of transforming measured scattering intensities $J(q(\theta))$ (in arbitrary units: counts/s) into values of $R(q(\theta))$ below:

1. *Volume Correction.* The photomultiplier "sees" different scattering volumes at different scattering angles. The measured intensity $J(q(\theta))$ must be corrected with a factor sin θ to give a volume-corrected scattering intensity $J_{sc}(q(\theta))$:

$$J_{sc}(q(\theta)) = J(q(\theta))\sin\theta \tag{17}$$

2. *Normalizing the Measured J_{sc} with a Reference Intensity.* The measured intensity is normalized with a reference intensity. The reference used is the intensity of the primary laser beam before it enters the scattering volume:

$$J_{norm}(q(\theta)) = J_{sc}(q(\theta))/I_0 \tag{18}$$

Since I_0 is also expressed in counts/s, $J_{norm}(q(\theta))$ is dimensionless.

3. *Calibration.* Values of $J_{norm}(q(\theta))$ are calibrated against $J_{norm,st}(q(\theta))$ of the standard scatterer toluene, of which the Rayleigh ratio R_{st} is precisely known.[39-41]

4. *Scattering of the Pure Solvent.* The (usually small) scattering ratio $J_{norm,sol}$ of the pure solvent has to be subtracted since we are interested in concentration fluctuations only. This ratio is measured separately.

Denoting the scattering ratio of the polymer solution by $J_{norm,pol}(q(\theta))$, the expression for the measured Rayleigh ratio $R(q(\theta))_m$ becomes

$$R(q(\theta))_m = \left[\frac{J_{norm,pol}(q)\left(\frac{n_s}{n_{st}}\right)^2 - J_{norm,sol}\left(\frac{n_{sol}}{n_{st}}\right)^2}{J_{norm,st}}\right]R_{st} \tag{19}$$

where n_s, n_{sol}, and n_{st} are refractive indices of solution, solvent, and standard, respectively. The terms $(n_s/n_{st})^2$ and $(n_{sol}/n_{st})^2$ are the refraction corrections to account for the fact that the scattered light is refracted at the liquid–glass interface.[42]

Table I. Composition and Temperature Region of the Samples

sample	wf2	error	T region (K)
I	5.04×10^{-3}	0.02×10^{-3}	298–404
II	1.60×10^{-2}	0.06×10^{-2}	301–400
III	3.25×10^{-2}	0.01×10^{-2}	301–401
IV	6.47×10^{-2}	0.04×10^{-2}	299–401
V	10.3×10^{-2}	0.1×10^{-2}	298–400

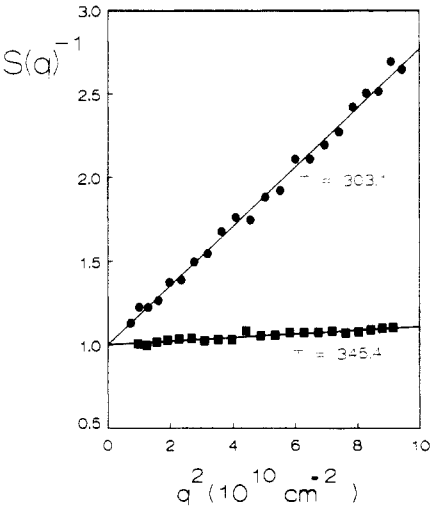

Figure 1. $S(q)^{-1}$ versus q^2 for sample III.

Sample Preparation. Methyl acetate ($CH_3CO_2CH_3$) was purchased from Aldrich Chemical Co. Inc. in a special anhydrous grade (water content < 0.005%). Methyl acetate was filtered for several hours in a closed filtration system through a 0.2-μm Millipore filter under a dry nitrogen atmosphere to remove dust particles. Polystyrene (M_w = 770 kg/mol; M_w/M_n = 1.04) was purchased from Polymer Labs, UK. A stock solution with a weight fraction of 5.04×10^{-3} was filtered through a 0.2-μm single-use Millipore filter. This is the lowest weight fraction used in the experiments. Samples with a higher weight fraction were prepared by heating the stock solution in the light scattering cuvette to evaporate methyl acetate. After evaporation the cuvette was refilled with a new amount of filtered mother solution and heated again. This procedure was continued until the desired weight fraction in the cuvette was reached. This weight fraction was calculated by accurately weighing the amounts of evaporated methyl acetate and the amounts of added stock solution.

Since light scattering experiments were carried out up to temperatures above the boiling point of methyl acetate, the quartz cuvettes were flame sealed, while the solution was frozen by keeping the bottom of the cuvettes immersed in liquid nitrogen. For this purpose the cuvettes were narrowed at the top, allowing them to be sealed quickly. As a consequence, experiments were carried out at an equilibrium liquid/vapor pressure that amounts to a 5-bar maximum, too small to influence the thermodynamic behavior.

Experiments were performed with five samples of different composition. In Table I we have listed the weight fraction wf2, the error in it, and the temperature region for which the sample could be used as determined by the cloud points of the samples.

Refractive Index Increments. Refractive index increments $(dn_s/dw)_T$ were measured with a differential refractometer, Model RF-600, manufactured by C. N. Wood Mfg. Co., Newton, PA. A 514.5-nm filter was used to match the wavelength of the laser light. $(dn_s/dw)_T$ data were measured for weight fractions up to 4% in a temperature range from 30 to 50 °C (values are limited by the measurement range of the refractometer). $(dn_s/dw)_T$ appeared to be constant over the whole concentration range and independent of temperature (which is not surprising, since the temperature dependence of dn_s/dc is mainly determined by the

Table II. Basic Light Scattering Results for Sample I

	0.504×10^{-2}					0.504×10^{-2}			
T (K)	$R(q(0))_m$ (10^{-3} cm^{-1})	ξ (nm)	$R(q(0))$ (10^{-3} cm^{-1})	$\partial^2\Delta G^V/\partial c^2$ (10^{-1} J m^3/kg^2)	T (K)	$R(q(0))_m$ (10^{-3} cm^{-1})	ξ (nm)	$R(q(0))$ (10^{-3} cm^{-1})	$\partial^2\Delta G^V/\partial c^2$ (10^{-1} J m^3/kg^2)
298.5	4.83	16.1	4.97	4.30	332.4	2.59	17.4	2.63	9.73
299.8					334.1	2.58	14.2	2.62	9.86
300.6	4.10	16.2	4.20	5.15	337.5	2.49	15.1	2.53	10.4
300.8					337.8	2.60	16.5	2.64	9.97
301.0					342.6	2.43	13.3	2.47	10.9
301.2					345.4	2.51	15.4	2.56	10.7
301.3					350.5	2.49	15.3	2.53	11.1
301.8	4.13	17.1	4.23	5.14	355.4	2.54	17.5	2.58	11.2
303.1	3.88	16.4	3.97	5.53	361.5	2.74	18.4	2.79	10.7
304.0	3.95	16.5	4.04	5.45	366.4				
305.2	3.60	16.5	3.68	6.03	373.3	2.80	18.9	2.85	11.1
306.9	3.35	15.4	3.42	6.55	378.9	2.77	16.1	2.81	11.6
309.6					382.4	2.96	16.5	3.01	11.0
310.0	3.34	15.8	3.41	6.68	388.0	3.17	19.8	3.22	10.5
311.2	2.93	17.1	2.98	7.69	393.4	3.43	18.0	3.50	10.0
312.6	3.06	16.1	3.12	7.39	398.0	4.18	16.5	4.29	8.33
314.8	2.74	16.5	2.77	8.44	399.6	4.25	19.2	4.36	8.26
318.4	2.82	15.2	2.87	8.30	400.5	4.23	19.4	4.33	8.37
318.8	3.21	15.8	3.28	7.29	401.3	4.20	17.5	4.30	8.45
323.4	2.80	17.3	2.85	8.57	403.9	5.59	19.0	5.77	6.37
327.2	2.61	14.1	2.66	9.36					

Table III. Basic Light Scattering Results for Sample II

	1.60×10^{-2}					1.60×10^{-2}			
T (K)	$R(q(0))_m$ (10^{-3} cm^{-1})	ξ (nm)	$R(q(0))$ (10^{-3} cm^{-1})	$\partial^2\Delta G^V/\partial c^2$ (10^{-1} J m^3/kg^2)	T (K)	$R(q(0))_m$ (10^{-3} cm^{-1})	ξ (nm)	$R(q(0))$ (10^{-3} cm^{-1})	$\partial^2\Delta G^V/\partial c^2$ (10^{-1} J m^3/kg^2)
298.5					332.4	7.04	16.8	7.34	3.48
299.8					334.1	7.13	14.7	7.45	3.46
300.6					337.5	6.42	14.3	6.68	3.93
300.8	49.2	36.3	64.1	0.34	337.8	6.21	13.3	6.45	4.06
301.0	47.9	33.3	62.9	0.34	342.6	6.43	13.6	6.69	4.03
301.2	38.5	31.8	47.5	0.46	345.4	6.02	12.5	6.25	4.37
301.3	39.6	31.7	49.4	0.44	350.5	6.50	14.6	6.76	4.14
301.8	29.8	28.1	35.2	0.62	355.4	6.47	16.2	6.73	4.27
303.1	25.2	24.4	29.3	0.75	361.5	6.96	17.5	7.26	4.08
304.0	22.5	23.5	25.7	0.86	366.4	7.25	14.4	7.59	4.00
305.2	20.0	21.8	22.6	0.98	373.3	7.57	16.8	7.93	3.96
306.9	15.6	19.8	17.1	1.31	378.9	8.38	16.3	8.81	3.66
309.6	12.7	18.6	13.7	1.64	382.4	9.40	16.7	9.96	3.31
310.0	13.9	18.2	15.2	1.49	388.0	10.8	19.1	11.5	2.93
311.2	11.8	17.1	12.7	1.79	393.4	13.9	19.9	15.1	2.31
312.6	11.2	17.9	12.0	1.91	398.0	32.8	25.7	40.0	0.89
314.8	9.27	17.0	9.80	2.38	399.6	37.3	31.9	45.7	0.78
318.4	9.61	16.3	10.2	2.32	400.5				
318.8					401.3				
323.4	7.83	15.0	8.22	2.97	403.9				
327.2	7.29	13.6	7.63	3.27					

thermal expansion of methyl acetate, which disappears again in dn_s/dw):

$$\left(\frac{dn_s}{dw}\right)_T = \left(\frac{dn_s}{dw}\right) = 0.2066 \pm 0.0005 \quad (20)$$

Using a density of methyl acetate of 930 kg/m^3, we obtain a value for dn_s/dc of 0.22 cm^3/g, in good agreement with the value measured by Chu et al.[31] The absolute value of the refractive index of the solution depends on temperature and on weight fraction of polystyrene. Hence, we write

$$n_s(T,w) = n_{sol}(T_0) + \left(\frac{dn_{sol}}{dT}\right)(T - T_0) + \left(\frac{dn_s}{dw}\right)_T w \quad (21)$$

For methyl acetate as the solvent, we use $n_{sol}(T_0) = 1.3637$, $T_0 = 300$ K, and $dn_{sol}/dT = -5 \times 10^{-4}$ K^{-1}.[44]

The final conversion of Rayleigh ratios $R(q(0))$ as a function of weight fraction of polymer to values of $\partial^2\Delta G^V/\partial c^2$ (eq 7) makes it necessary to calculate values for dn_s/dc:

$$\frac{dn_s}{dc} = \frac{dn_s}{dw}\left(\frac{dc(w)}{dw}\right)^{-1} \quad (22)$$

where $c(w)$ is given by

$$c(w) = \frac{w}{w/\rho_p + (1-w)/\rho_s} \quad (23)$$

For the density of polystyrene, ρ_p (in kg/m^3), we use[43]

$$\rho(T) = 1089 - 0.6458(T - 273.15) \quad (24)$$

and the density of methyl acetate ρ_s, is given by[44]

$$\rho_s = 927.3 - 1.3(T - 298.15) \quad (25)$$

The conversion, eq 22, leads to a minor concentration dependence of dn_s/dc values.

Results

Light Scattering Data. In Figure 1 we show plots of measured structure factors $S(q)^{-1} = R(q(0))/R(q(\theta))$ versus q^2 for sample III at two different temperatures. One temperature is nearly critical (close to the UCST) and hence ξ is large. The other temperature is chosen just between UCST and LCST, where ξ has become much smaller. At this temperature, the order of magnitude of

Table IV. Basic Light Scattering Results for Sample III

	3.25×10^{-2}					3.25×10^{-2}			
T (K)	$R(q(0))_m$ (10^{-3} cm^{-1})	ξ (nm)	$R(q(0))$ (10^{-3} cm^{-1})	$\partial^2\Delta G^V/\partial c^2$ (10^{-1} J m^3/kg^2)	T (K)	$R(q(0))_m$ (10^{-3} cm^{-1})	ξ (nm)	$R(q(0))$ (10^{-3} cm^{-1})	$\partial^2\Delta G^V/\partial c^2$ (10^{-1} J m^3/kg^2)
298.5					332.4	9.35	13.9	9.92	2.56
299.8					334.1	9.04	9.8	9.60	2.67
300.6					337.5	8.43	11.5	8.90	2.94
300.8					337.8	8.99	11.7	9.53	2.73
301.0					342.6	8.59	12.4	9.08	2.94
301.2					345.4	8.07	10.2	8.51	3.18
301.3					350.5	8.65	13.1	9.14	3.05
301.8					355.4	8.71	14.2	9.20	3.10
303.1	102.0	42.0	227.0	0.10	361.5	8.71	13.7	9.20	3.20
304.0	68.9	33.5	112.0	0.20	366.4	9.58	12.7	10.2	2.96
305.2	58.4	30.3	87.0	0.25	373.3	10.8	14.9	11.5	2.71
306.9	34.3	22.8	42.9	0.52	378.9	11.4	13.4	12.3	2.61
309.6	24.5	19.3	28.7	0.79	382.4	13.6	14.1	14.9	2.19
310.0	26.3	18.9	31.3	0.72	388.0	16.6	17.3	18.5	1.81
311.2	20.7	17.4	23.6	0.97	393.4	25.0	21.1	29.2	1.18
312.6	19.3	16.9	21.8	1.05	398.0	82.5	33.8	176.0	0.20
314.8	15.8	16.5	17.4	1.33	399.6				
318.4	14.0	14.5	15.3	1.57	400.5	105.0	50.5	199.0	0.18
318.8					401.3				
323.4	11.6	13.1	12.5	1.94	403.9				
327.2	9.98	11.0	10.7	2.32					

Table V. Basic Light Scattering Results for Sample IV

	6.47×10^{-2}					6.47×10^{-2}			
T (K)	$R(q(0))_m$ (10^{-3} cm^{-1})	ξ (nm)	$R(q(0))$ (10^{-3} cm^{-1})	$\partial^2\Delta G^V/\partial c^2$ (10^{-1} J m^3/kg^2)	T (K)	$R(q(0))_m$ (10^{-3} cm^{-1})	ξ (nm)	$R(q(0))$ (10^{-3} cm^{-1})	$\partial^2\Delta G^V/\partial c^2$ (10^{-1} J m^3/kg^2)
298.5					332.4				
299.8					334.1	8.69	7.6	9.22	2.75
300.6	68.9	28.8	123	0.17	337.5				
300.8					337.8	7.75	7.6	8.16	3.16
301.0	69.9	27.8	131	0.16	342.6				
301.2	62.2	27.9	100	0.21	345.4	7.17	6.9	7.52	3.57
301.3	64.5	27.1	110	0.20	350.5				
301.8	48.5	23.2	69.7	0.31	355.4				
303.1	39.4	18.4	53.2	0.41	361.5				
304.0	32.7	15.7	41.8	0.52	366.4	8.50	10.4	8.99	3.31
305.2	31.4	17.2	39.3	0.56	373.3	9.90	11.2	10.6	2.89
306.9	23.1	13.7	27.3	0.81	378.9	11.3	12.0	12.1	2.60
309.6	16.8	10.7	18.8	1.19	382.4	12.7	12.2	13.8	2.33
310.0	18.0	11.3	20.5	1.09	388.0	13.6	12.5	14.9	2.21
311.2	16.5	9.9	18.5	1.22	393.4	19.4	16.3	22.1	1.54
312.6	14.5	11.1	16.0	1.42	398.0				
314.8					399.6				
318.4	11.7	9.4	12.7	1.84	400.5	51.0	37.7	66.6	0.53
318.8					401.3				
323.4					403.9				
327.2									

ξ can be compared to that of a single polymer coil. It is obvious that for both conditions eq 10 holds quite well, as expected. This was the case for all other samples as well. Hence, we can apply the turbidity correction, eqs 15 and 16, unambiguously.

After extrapolation of all $R(q(\theta))_m$ data to $\theta = 0$ and determination of ξ values according to eq 10, the $R(q(0))_m$ data were corrected for turbidity by solving eq 16 (using Newton–Raphson iteration), where the internal diameter d of the cuvettes was measured to be 7.90 mm. Consequently, values for $\partial^2\Delta G^V/\partial c^2$ could be calculated using eq 7. Results for $R(q(0))_m$, ξ, $R(q(0))$, and $\partial^2\Delta G^V/\partial c^2$ for all five samples are listed in Tables II–VI.

The influence of turbidity is depicted in Figure 2, where the ratio $R(q(0))/R(q(0))_m$ is shown for the weakest scatterer, sample I, and for the strongest scatterer, sample III, as a function of temperature. For sample I, the ratio remains very close to unity at all temperatures, with a minor increase close to the binodals. For sample III, the correction amounts to approximately 5% at 350 K, just in between UCST and LCST, and increases strongly close to the binodals.

All turbidity-corrected Rayleigh ratios $R(q(0))$ have been plotted in Figure 3. The logarithmic scale is chosen for convenience only. Note that sample III, with a weight fraction of 3.25%, is the strongest scatterer at all temperatures. Note also that the temperature dependence of $R(q(0))$ is most pronounced for sample III. Apparently, of all concentrations, that of sample III is closest to both the upper and lower critical points of the solution.

The principal result of this work is shown in Figure 4, where the experimentally determined values of $\partial^2\Delta G^V/\partial c^2$ have been plotted. The free energy curvature is smallest for sample III (wf2 = 0.0325) and it is nearly zero at both the high- and the low-temperature side, indicating that the concentration of sample III is close to critical. Extrapolation of the data toward $\partial^2\Delta G^V/\partial c^2 = 0$ results in a UCST critical temperature of 301.5 K and an LCST critical point of 402.5 K.

Plots of the correlation lengths ξ are shown in Figure 5. For sample I, the lowest concentration (0.504%), ξ appears to be nearly independent of temperature. The isolated chain collapse at the upper and lower critical Θ temperatures, observed in very dilute solutions of poly-

Table VI. Basic Light Scattering Results for Sample V

	10.3×10^{-2}					10.3×10^{-2}			
T (K)	$R(q(0))_m$ (10^{-3} cm^{-1})	ξ (nm)	$R(q(0))$ (10^{-3} cm^{-1})	$\partial^2\Delta G^V/\partial c^2$ (10^{-1} J m^3/kg^2)	T (K)	$R(q(0))_m$ (10^{-3} cm^{-1})	ξ (nm)	$R(q(0))$ (10^{-3} cm^{-1})	$\partial^2\Delta G^V/\partial c^2$ (10^{-1} J m^3/kg^2)
298.5	19.9	12.5	22.8	0.92	332.4				
299.8	15.5	11.2	17.2	1.22	334.1	5.71	9.6	5.93	4.22
300.6	15.3	10.5	17.0	1.25	337.5				
300.8					337.8	4.00	6.9	5.07	5.02
301.0					342.6				
301.2					345.4	4.87	7.8	5.02	5.27
301.3					350.5				
301.8	13.3	9.7	14.6	1.45	355.4				
303.1	13.0	9.6	14.3	1.49	361.5				
304.0	11.4	9.5	12.3	1.74	366.4	5.03	9.2	5.19	5.62
305.2	11.6	11.3	12.5	1.74	373.3	6.05	8.0	6.30	4.79
306.9	9.44	9.0	10.0	2.18	378.9	6.70	8.0	7.0	4.42
309.6	8.88	8.0	9.43	2.34	382.4	6.78	10.2	7.08	4.45
310.0	9.36	9.6	10.0	1.22	388.0	7.81	10.6	8.22	3.95
311.2	9.19	9.6	9.77	2.27	393.4	10.3	13.2	10.9	3.04
312.6	6.21	8.8	6.47	3.52	398.0	18.5	17.1	20.8	1.63
314.8					399.6	17.9	15.0	20.1	1.69
318.4					400.5				
318.8					401.3				
323.4					403.9				
327.2									

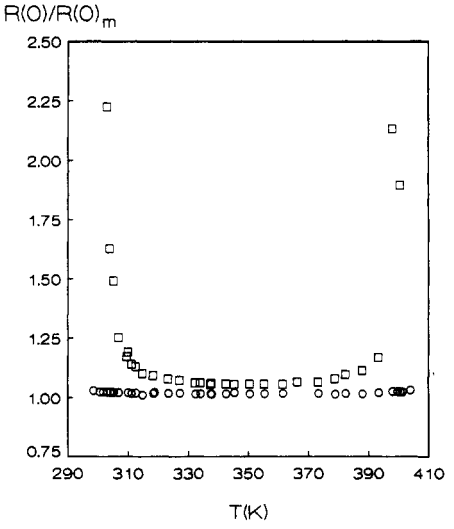

Figure 2. Ratio $R(q(0))/R(q(0))_m$ versus temperature for samples I (dots) and III (squares).

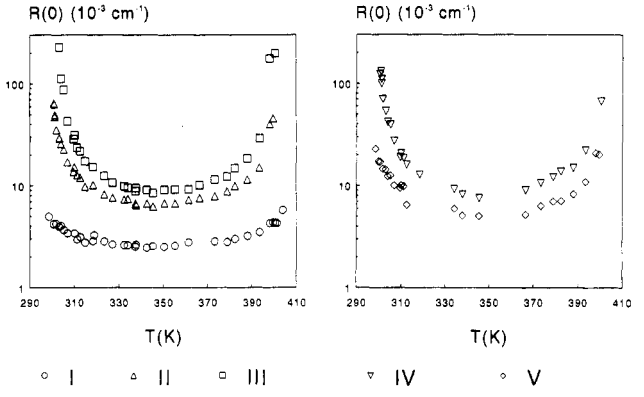

Figure 3. $R(q(0))$ versus temperature for samples I–V.

styrene in methyl acetate,[31] cannot be observed anymore at this concentration. At higher concentrations, correlation lengths appear to increase close to the binodals, as observed in the $R(q(0))$. Again, this effect is most pronounced for the "critical" concentration, sample III.

It is interesting to note that, for all five samples, the correlation length ξ appears to be rather constant in the temperature range between 330 and 370 K. In Figure 6 we have plotted the average value of ξ in this temperature range as a function of concentration. ξ appears to decrease with increasing concentration.

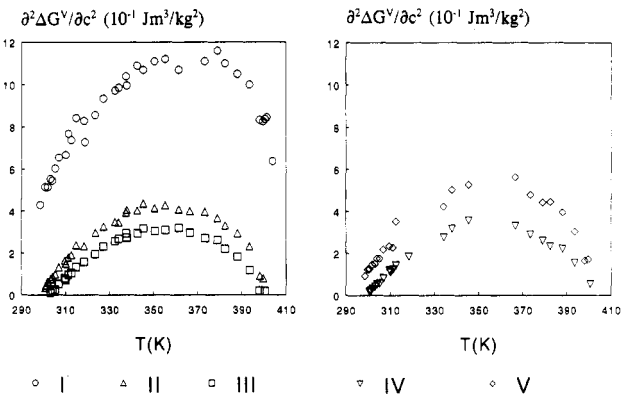

Figure 4. Experimentally determined values of $\partial^2(\Delta G^V)/\partial c^2$ for samples I–V.

Binodals. The binodals (cloud points) of the solution could be observed easily: Once phase separation had set in, the solution immediately became "cloudy", and the laser beam was no longer able to pass through the sample. By repetitive slow cooling and heating, binodals could be determined with an accuracy of 0.1 K. Results are shown in Figure 7.

Conclusions

By analyzing light scattering intensities, we have calculated values for the free energy curvature $\partial^2\Delta G^V/\partial c^2$ for the model polymer solution polystyrene in methyl acetate. This has been done in the homogeneous one-phase region of this system from dilute to moderate concentrations and from 300 to 400 K. Similar and extensive data have been obtained by, e.g., Scholte[45] and references therein. Correlation lengths, together with binodals, were determined as well.

To generate the data mentioned above, it was necessary to handle the large scattering intensities (turbidity) of critical and concentrated polymer solutions. We developed a numerical procedure to calculate the actual forward scattered intensity $R(q(0))$ from the measured forward scattered intensity $R(q(0))_m$ and the correlation length, ξ, which completely characterizes the angular dependence. This method can be applied to every system in which

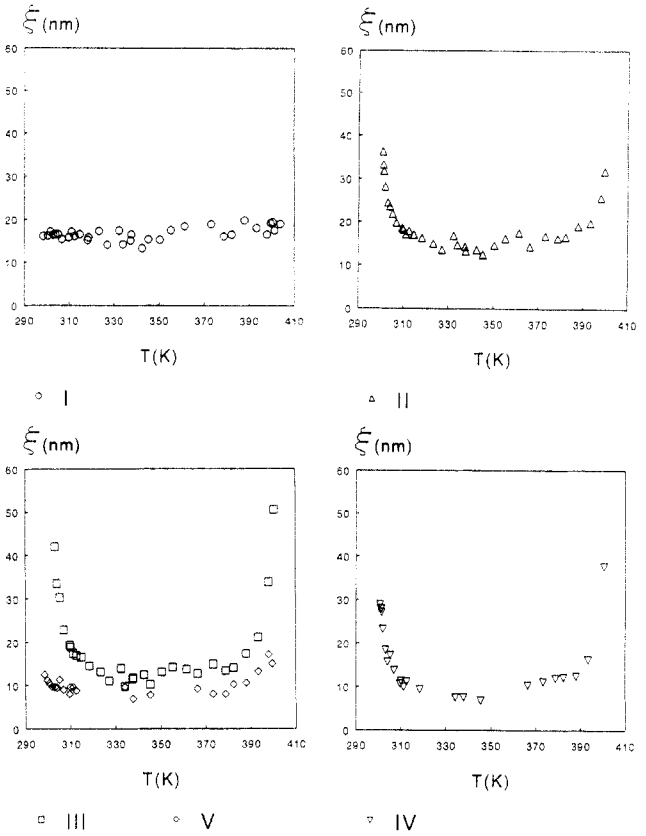

Figure 5. Correlation lengths ξ versus temperature for samples I–V.

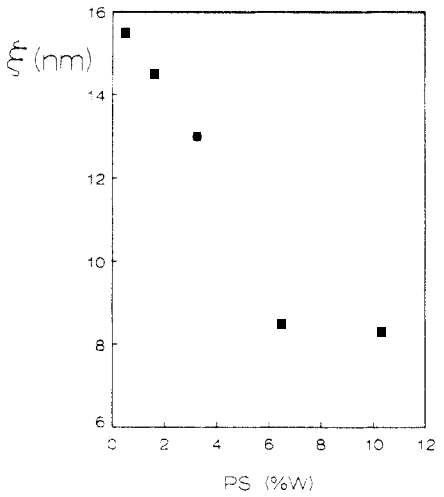

Figure 6. Average value of ξ between 330 and 370 K versus concentration.

turbidity, i.e., a measurable attenuation of the laser beam inside the scattering liquid, plays a role.

Besides the fact that the free energy curvature changes with temperature and concentration, we have also observed that the average "structure" of the solution changes: correlation lengths ξ increase close to spinodals, and in between UCST and LCST, "structure" seems to disappear with increasing concentration. It should be noted that these types of structural changes are not incorporated in any mean field theory, where polymer chains are modeled essentially as Gaussian coils, containing no net internal entropy of mixing.

The experimentally obtained values of $\partial^2 \Delta G^V / \partial c^2$ as a function of concentration and temperature call for a comparison with theoretical predictions. Unfortunately, there is currently no truly predictive theory that could

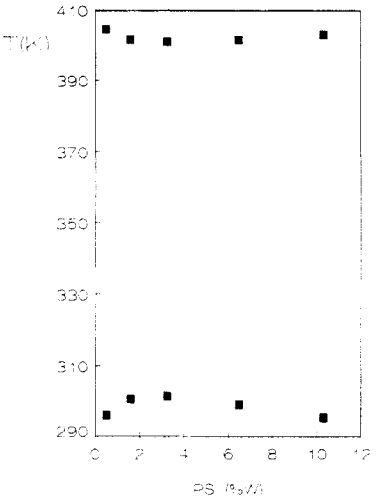

Figure 7. Cloud points of polystyrene in methyl acetate.

thus be tested. As discussed, many theories have been developed by various groups, based on contributions to ΔG from chain configurational effects, dispersive and specific interactions, and compressibility effects. However, each theory requires experimental data on the phase behavior to fit empirical parameters in the theory. Since, in our opinion, there is no strong reason to prefer any one of these theories to the others, we have left the task of comparing our experimental data with these theories to another occasion. For ease of comparison, the experimental data have also been presented in tabular form.

References and Notes

(1) Flory, P. J. *J. Chem. Phys.* **1941**, *9*, 660.
(2) Flory, P. J. *J. Chem. Phys.* **1942**, *10*, 51.
(3) Huggins, M. L. *J. Chem. Phys.* **1941**, *9*, 440.
(4) Huggins, M. L. *J. Phys. Chem.* **1942**, *46*, 151.
(5) Huggins, M. L. *Ann. N.Y. Acad. Sci.* **1942**, *41*, 1.
(6) Rehage, G.; Moeller, D. *J. Polym. Sci., Polym. Symp.* **1967**, *16*, 1787.
(7) Siow, K. S. Delmas, G.; Patterson, D. *Macromolecules* **1972**, *5*, 29.
(8) Krause, S.; Stroud, D. E. *J. Polym. Sci., Polym. Phys. Ed.* **1973**, *11*, 2253.
(9) Kuwahara, N.; Nakata, M.; Kanako, M. *Polymer* **1973**, *14*, 415.
(10) Saeki, S.; Kuwahara, N.; Konno, S.; Kaneko, M. *Macromolecules* **1973**, *6*, 246.
(11) Saeki, S.; Konno, S.; Kuwahara, N.; Nakata, M.; Kaneko, M. *Macromolecules* **1974**, *7*, 521.
(12) Koningsveld, R. *Br. Polym. J.* **1975**, *7*, 435.
(13) Einaga, Y.; Ohsahi, S.; Tong, Z.; Fujita, H. *Macromolecules* **1984**, *17*, 527.
(14) Raetzsch, M. T.; Krueger, B.; Kehlen, H. *J. Macromol. Sci., Chem.* **1990**, *27*, 683.
(15) Koningsveld, R.; Kleintjes, L. A.; Schultz, A. R. *J. Polym. Sci.* **1970**, *8*, 1261.
(16) Derham, K. W.; Goldsbrough, J.; Gordon, M. *Pure Appl. Chem.* **1974**, *38*, 97.
(17) Irvine, P.; Gordon, M. *Macromolecules* **1980**, *13*, 761.
(18) Kiepen, F.; Burchard, W. *Macromolecules* **1988**, *21*, 1784.
(19) Prigogine, I.; Bellemans, A.; Mathot, V. *The Molecular Theory of Solutions*; North-Holland Publishing Co.: Amsterdam, 1957.
(20) Flory, P. J.; Orwoll, R. A.; Vrij, A. *J. Am. Chem. Soc.* **1964**, *86*, 3567.
(21) Sanchez, I. C.; Lacombe, R. U. *J. Phys. Chem.* **1976**, *80*, 2352.
(22) Kleintjes, L. A.; Koningsveld, R. *Colloid Interface Sci.* **1980**, *258*, 711.
(23) Stroeks, A.; Nies, E. *Polym. Eng. Sci.* **1988**, *28*, 1347.
(24) Nies, E.; Stroeks, A. *Macromolecules* **1990**, *23*, 4088.
(25) Stroeks, A.; Nies, E. *Macromolecules* **1990**, *23*, 4092.
(26) Nies, E.; Stroeks, A.; Simha, R.; Jain, R. K. *Colloid Polym. Sci.* **1990**, *268*, 731.
(27) Ten Brinke, G.; Karasz, F. E. *Macromolecules* **1984**, *17*, 815.

(28) Painter, P. C.; Graf, J.; Coleman, M. M. *J. Chem. Phys.* **1990**, *29*, 6166.
(29) Wakker, A. *Polymer* **1991**, *32*, 279.
(30) Sanchez, I. C.; Balazs, A. C. *Macromolecules* **1989**, *22*, 2325.
(31) Chu, B.; Park, I. H.; Wang, Q. W.; Wu, C. *Macromolecules* **1987**, *20*, 2833.
(32) Kubota, K.; Abbay, K. M.; Chu, B. *Macromolecules* **1983**, *16*, 137.
(33) Burchard, W. *Adv. Polym. Sci.* **1983**, *48*, 1.
(34) Einstein, A. *Ann. Phys. (Leipzig)* **1910**, *33*, 1275.
(35) von Smoluchowski, M. *Ann. Phys. (Leipzig)* **1908**, *25*, 205.
(36) Stanley, H. E. *Phase Transitions and Critical Phenomena*; Oxford University Press: Oxford, 1971.
(37) Shanks, J. G.; Sengers, J. V. *Phys. Rev. A* **1988**, *38*, 885.
(38) Bantle, S.; Schmidt, M.; Burchard, W. *Macromolecules* **1982**, *15*, 1604.
(39) Cantow, H. J. *Makromol. Chem.* **1956**, *19*, 367.
(40) Pike, E. R.; Pomeroy, W. R. M.; Vaughan, J. M. *J. Chem. Phys.* **1975**, *62*, 3188.
(41) Bender, T. M.; Lewis, R. J.; Pecora, R. *Macromolecules* **1986**, *19*, 244.
(42) Hermans, J. J.; Levinson, S. *J. Opt. Soc. Am.* **1951**, *41*, 1033.
(43) Zoller, P. *Kunststoffe* **1976**, *66*, 363.
(44) Huglin, M. B. *Light Scattering from Polymer Solutions*; Academic Press: London, 1972.
(45) Scholte, Th.G. *J. Polym. Sci.* **1972**, *39*, 281.